SUPPORTING INFORMATION

for

Plasmonic Enhancement of Semiconducting Double Cable Polythiophene-Perylene Diimide Polymer Performance in Artificial Photosynthesis of H2O2

Faseeh Akbar†[a], Shahryar Rasheed[a], Sana Iqbal[a], Shiza Basit[a], Sumera Siddique[b], Ishtiaq Ahmed[c], Ljiljana Fruk[c], and Basit Yameen[a]*

*E-mail: basit.yameen@lums.edu.pk

[a] Department of Chemistry and Chemical Engineering, Syed Babar Ali School of Science and Engineering (SBASSE), Lahore University of Management Sciences (LUMS), Lahore-54792, Pakistan.

[b] Department of Physics, Syed Babar Ali School of Science and Engineering (SBASSE), Lahore University of Management Sciences (LUMS), Lahore-54792, Pakistan.

[c] Department of Chemical Engineering and Biotechnology, University of Cambridge. Philippa Fawcett Drive, CB3 0AS Cambridge, UK.

KEYWORDS: Artificial photosynthesis, Semiconducting polymers, Plasmonic nanoparticle, Double-cable polymers, Photocatalysis, Solar fuels.

Contents

1. Scheme, Spectra, Structures and Figures/Images

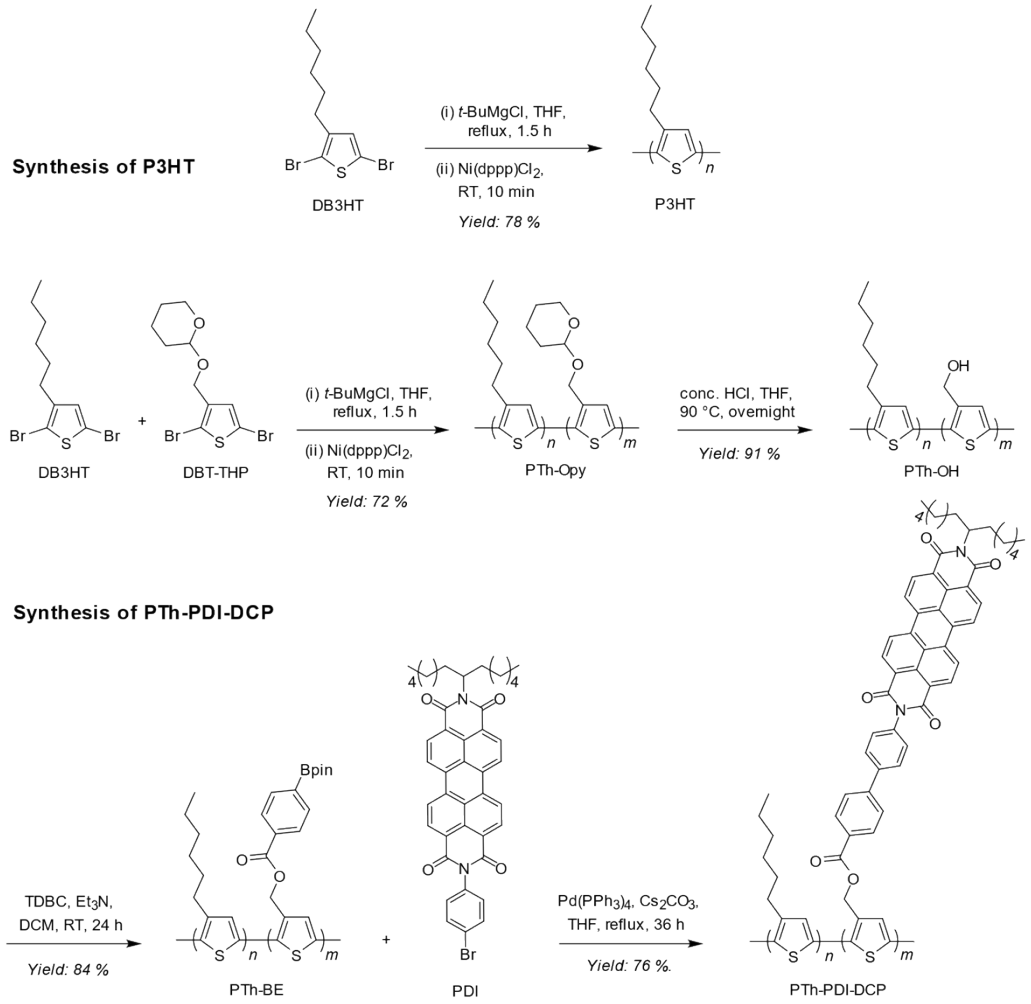

Scheme S1 Synthetic route for the preparation of poly-3-hexylthiophene (P3HT) and the donor-acceptor covalent conjugate (PTh-PDI-DCP).

2. Characterizations (GPC, ATR-FTIR and ^{1}H NMR)

Gel permeation chromatography (GPC) confirmed the incorporation of perylene diimide (PDI) units onto the side chains of the polythiophene (PTh) backbone as evidenced by increased molecular weight and lower retention time of PTh-PDI-DCP. The number average molecular weight (M_n) evolved from 6,700 Da ($Đ$ = 1.10) for PTh-Opy to 6,200 Da ($Đ$ = 1.05) after removal of -Opy groups (PTh-OH) followed by an increase to 7,900 Da ($Đ$ = 1.05) for PTh-BE and 10,900 Da ($Đ$ = 1.07) for PTh-PDI-DCP confirming successful grafting of PDI units (Fig. S1a). ATR-FTIR spectroscopy further supported functionalization with characteristic PDI bands at 1690 and 1610 cm^{-1} corresponding to amide C=O stretching and aromatic C=C vibrations, respectively (Fig. S1b). The ^{1}H NMR spectra of P3HT and PDI displayed their characteristic signals. For P3HT, the thiophene proton h appears at 6.9 ppm, the α-alkyl protons f at 2.8 ppm and remaining alkyl protons a-e at 0.7-1.9 ppm (Fig. S1c). PDI shows aromatic protons at 7-9 ppm, a methine proton r at 5.2 ppm and alkyl chain protons at 0.8-2.3 ppm (Fig. S1d). The ^{1}H NMR spectrum of PTh-PDI-DCP further confirms PDI incorporation with characteristic aromatic signals (δ = 7.5-9.0 ppm). Signal integration indicates ~13% functionalization of PTh side chains with PDI units (Fig. S1e, *detailed discussion provided in the main manuscript*).

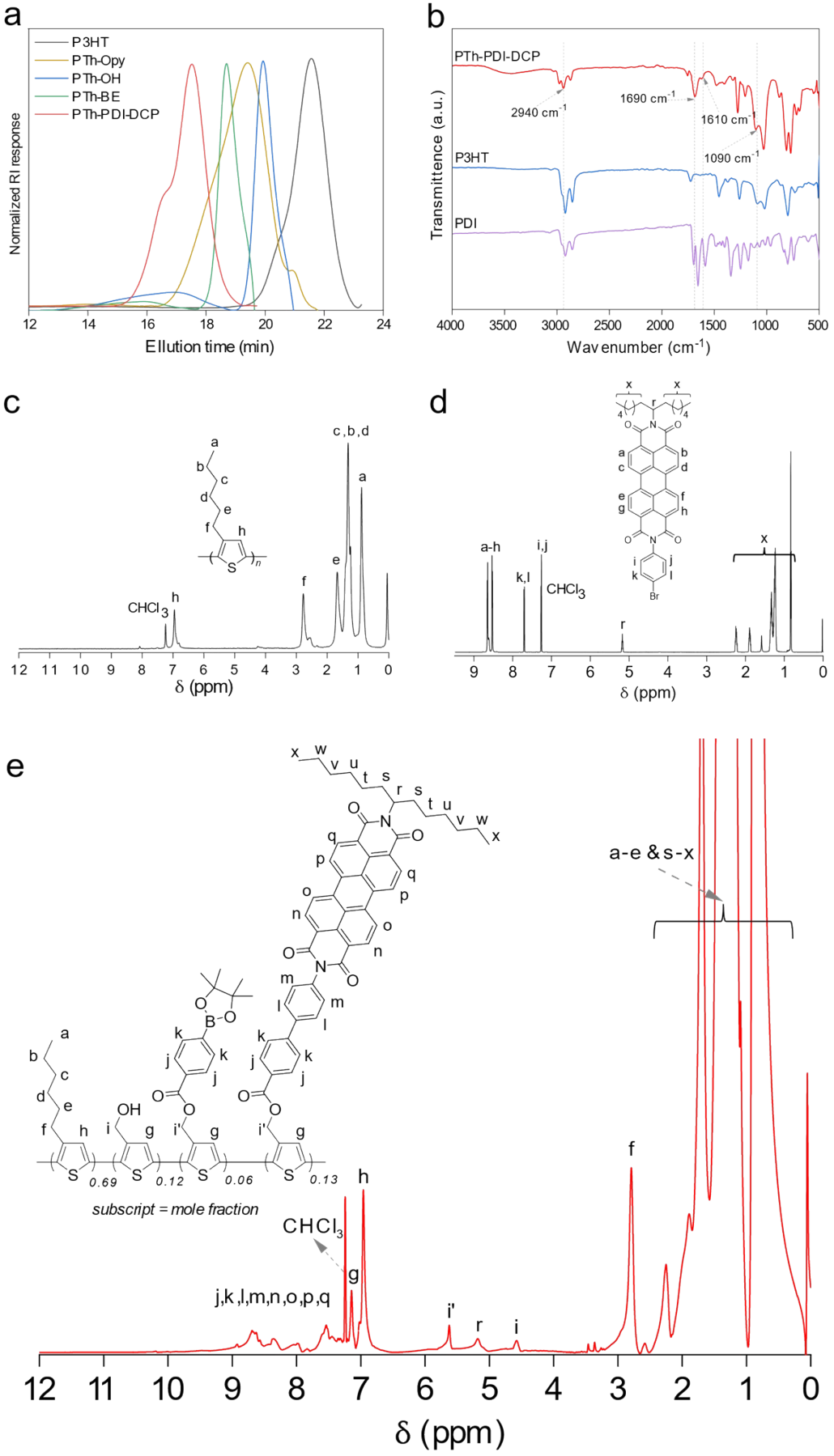

Fig. S1 (a) GPC profiles; (b) ATR-FTIR spectra of P3HT, PDI and PTh-PDI-DCP; (c, d, e) ^{1}H NMR spectra; P3HT (c), PDI (d) and PTh-PDI-DCP (e).

3. Band-gap calculations

The optical band gaps of PTh and PDI were determined by constructing Tauc plots derived from their corresponding UV/Vis absorption spectra. The frontier molecular orbital (FMO) energy levels were estimated through cyclic voltammetry (CV) measurements with all potentials referencSed against the ferrocene/ferrocenium (Fc/Fc^{+}) redox couple as an internal standard. The HOMO energy levels were calculated using Eq. S1 while the LUMO energy levels were determined using Eq. S2. The UV/Vis absorption spectra, Tauc plots and cyclic voltammograms of PTh and PDI are presented in Fig. S2.

$$E_{HOMO} = -\left[\left(P_{oxi\ compound} - P_{red}\frac{Fc}{Fc} + \right) + 4.8\right]eV \quad \text{..... Eq. S1}$$

$$E_{HOMO} = ELUMO - E_g \quad \text{..... Eq. S2}$$

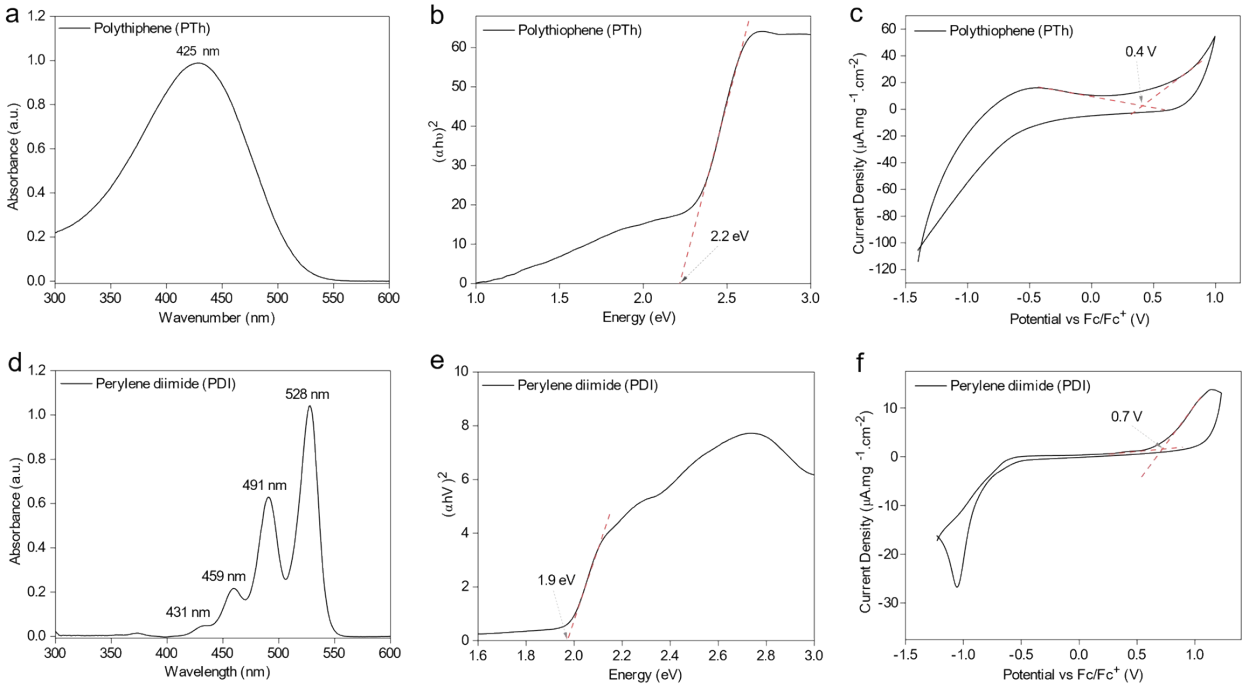

Fig. S2 (a, b, c) UV/Visible spectrum, Tauc plot and cyclic voltammogram of polythiophene (PTh); (d, e, f) UV/Visible spectrum, Tauc plot and cyclic voltammogram of perylene diimide (PDI).

Table S1 Summary of the amount of AuNPs transferred to the polymer solution upon addition of different volumes of AuNP suspension and their corresponding content in the polymer/AuNP hybrids. Amounts of Au were estimated using ICP-OES.

Serial no.	Volume of AuNPs suspensions (mL) with corresponding masses (mg) of AuNPs	Amount of AuNPs transferred to P3HT (mg)	Wt.% of AuNPs in P3HT/AuNPs hybrid	Amount of AuNPs transferred to PTh-PDI-DCP (mg)	Wt.% of AuNPs in PTh-PDI-DCP/AuNPs hybrid
1	5.0 mL / 2.3 mg	0.03 ± 0.01	3 ±1	0.10 ± 0.01	9 ±1
2	7.5 mL / 3.4 mg	0.06 ± 0.015	6 ±1.5	0.12 ± 0.01	11 ±1
3	10.0 mL / 4.5 mg	0.12 ± 0.01	10 ±1	0.15 ± 0.01	13 ±1
4	12.5 mL / 5.6 mg	0.19 ± 0.04	16 ±3	0.23 ± 0.025	19 ±3
5	15.0 mL /6.7 mg	0.24 ± 0.03	19 ±2.5	0.33 ± 0.03	25 ±3

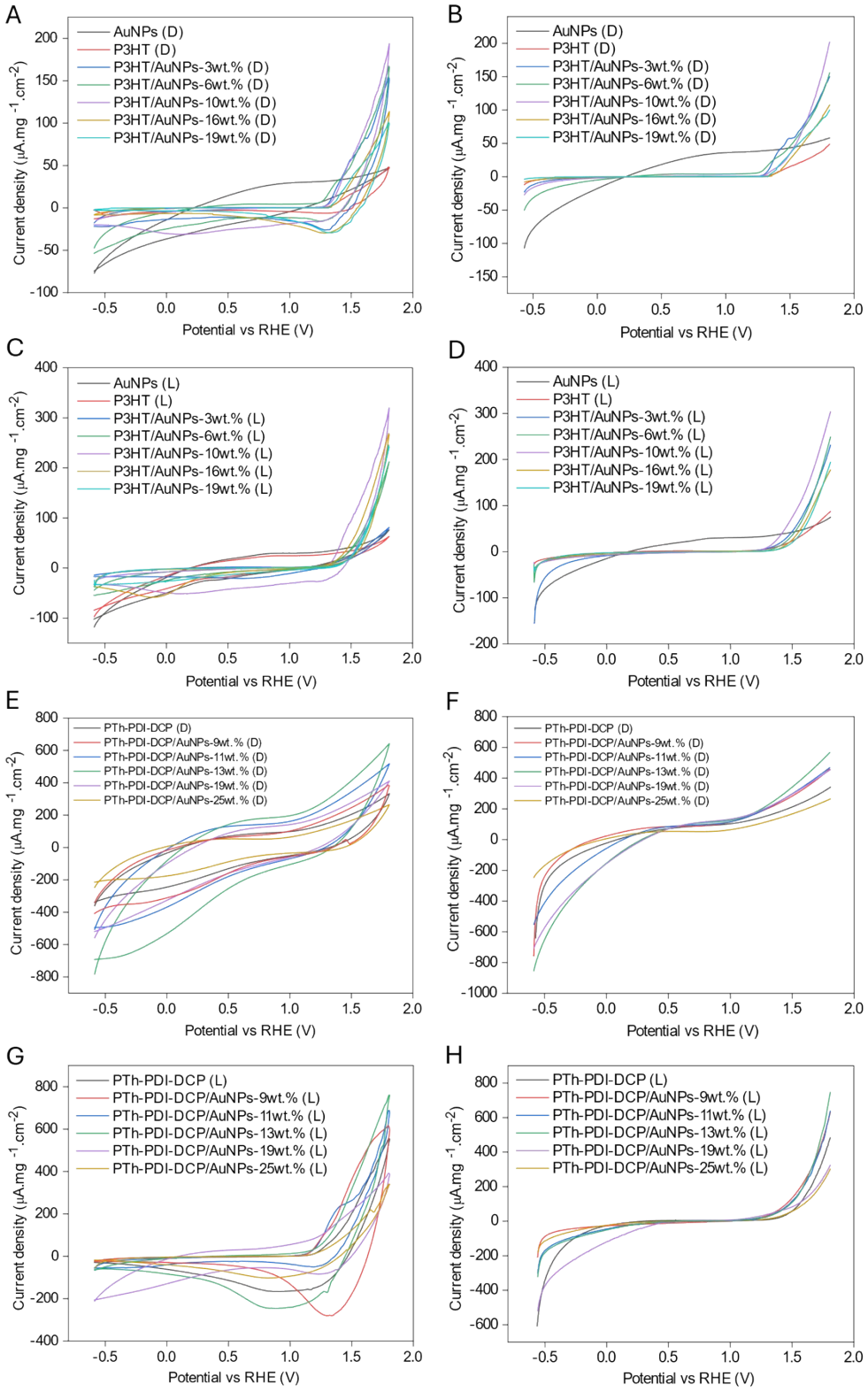

Fig. S3 Photoelectrochemical (PEC) performance of P3HT and PTh-PDI-DCP with varying AuNP wt.%. Cyclic voltammograms (CVs) (A) and linear sweep voltammograms (LSVs) (B) of AuNPs, pristine P3HT and P3HT/AuNP hybrids with different AuNP loadings (wt.%) recorded under dark conditions; CVs (C) and LSVs (D) of the same systems under illumination. CVs (E) and LSVs (F) of pristine PTh-PDI-DCP and PTh-PDI-DCP/AuNP hybrids with varying AuNP content (wt.%) measured in the dark; CVs (G) and LSVs (H) of the corresponding systems under illumination.

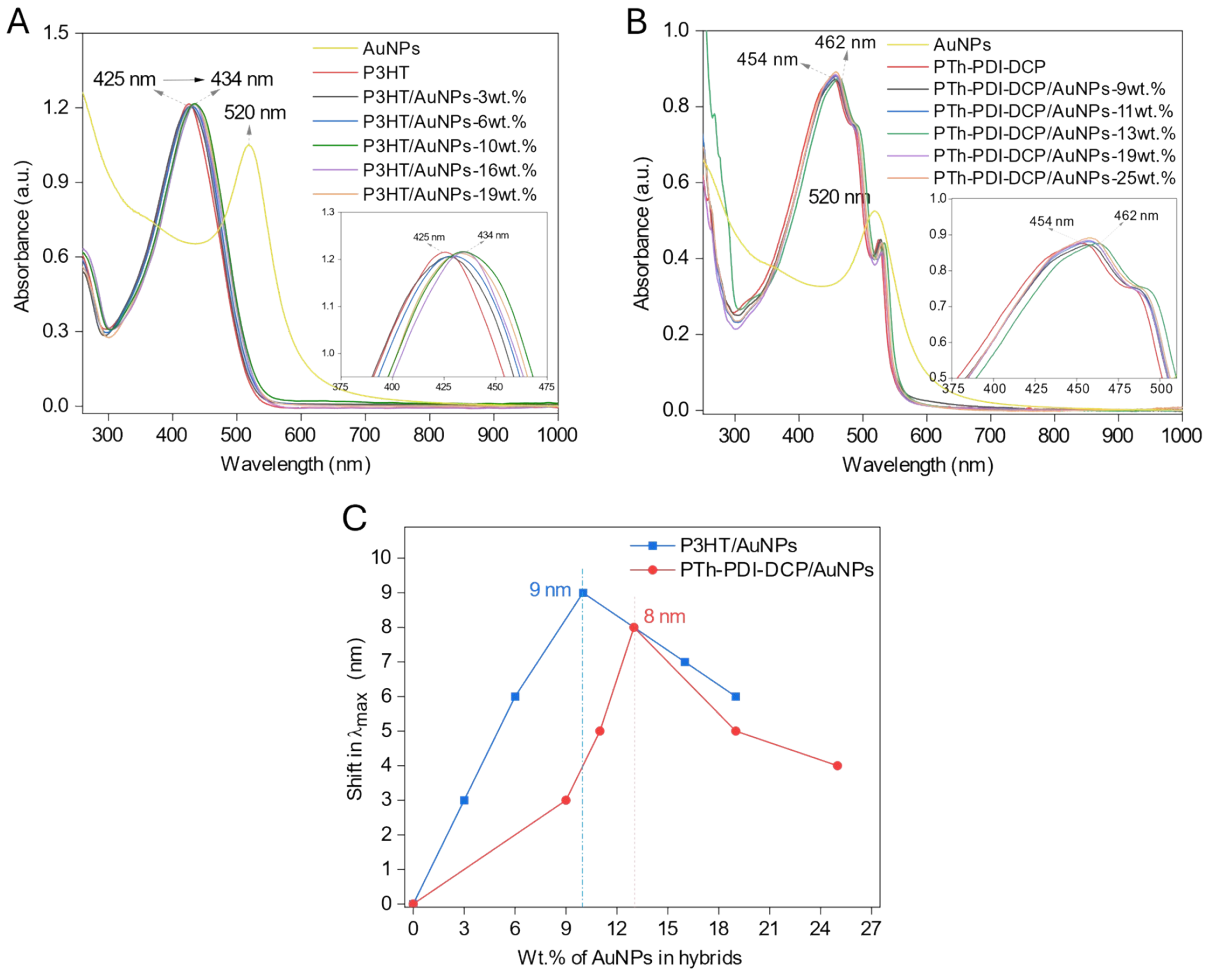

Fig. S4 UV/Visible absorption spectra of P3HT/AuNP hybrids (A) and PTh-PDI-DCP/AuNP hybrids (B), along with the corresponding shift in λ_{max} extracted from the UV/visible spectra of polymer/AuNP hybrids as a function of variable AuNP wt.% (C).

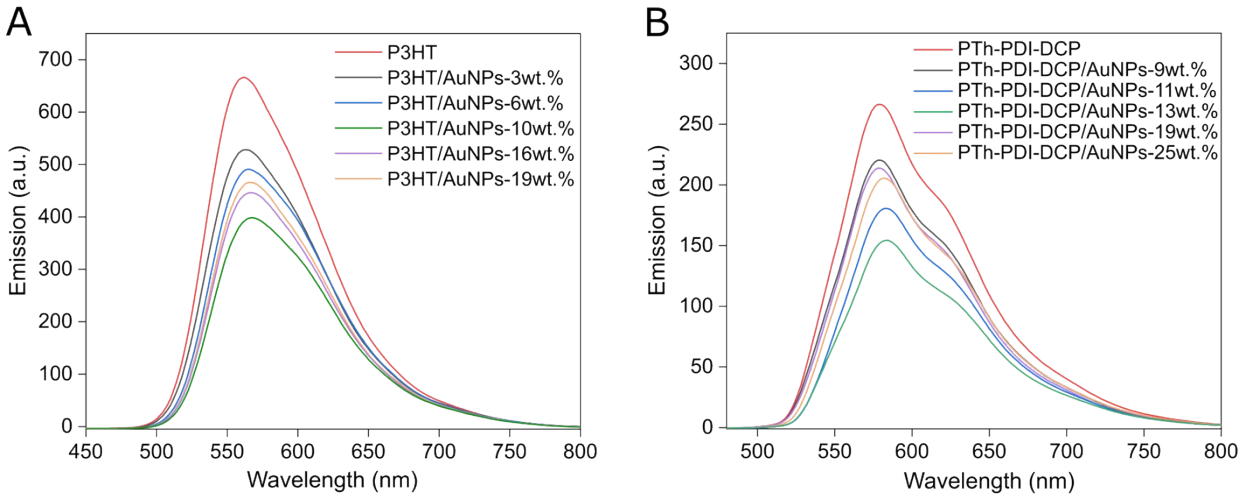

Fig. S5 Steady-state photoluminescence (PL) spectra of (A) P3HT and P3HT/AuNP hybrids with varying AuNP weight percentages (wt.%) and (B) PTh-PDI-DCP and PTh-PDI-DCP/AuNP hybrids with different AuNP contents (wt.%) in the polymer/AuNP hybrid systems.

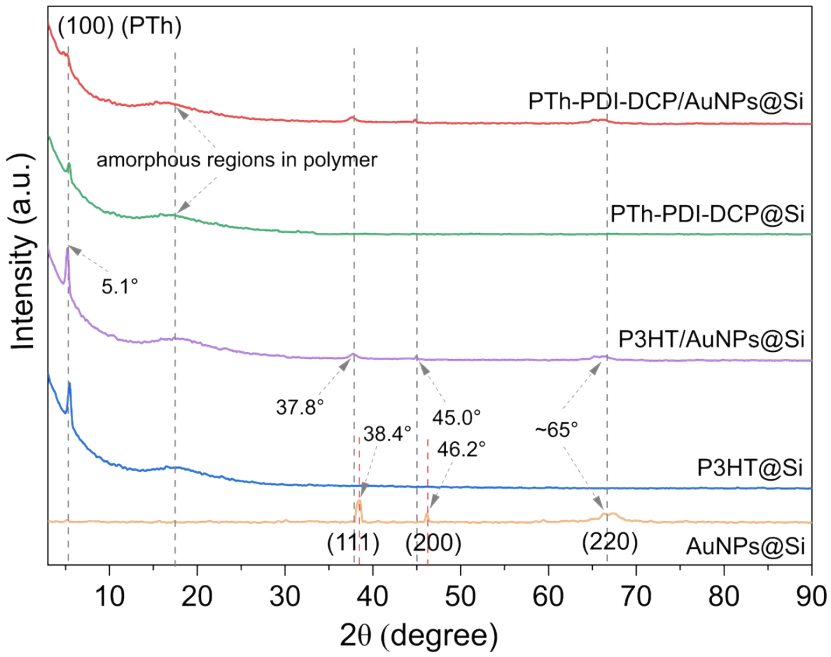

Fig. S6 GI-XRD patterns of AuNPs, P3HT and PTh-PDI-DCP, P3HT/AuNPs and PTh-PDI-DCP/AuNPs films deposited on Si wafers.

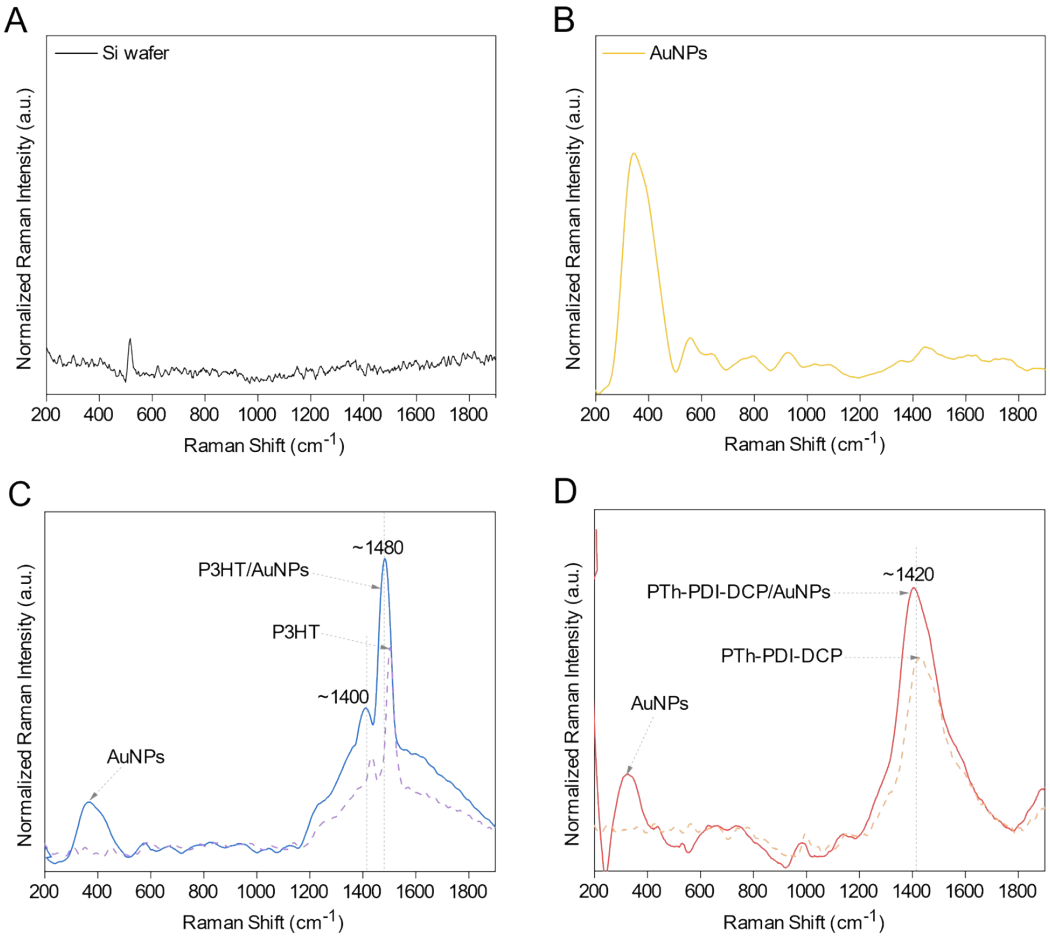

Fig. S7 Raman spectra of AuNPs, P3HT, P3HT/AuNPs, PTh-PDI-DCP and PTh-PDI-DCP/AuNPs films.

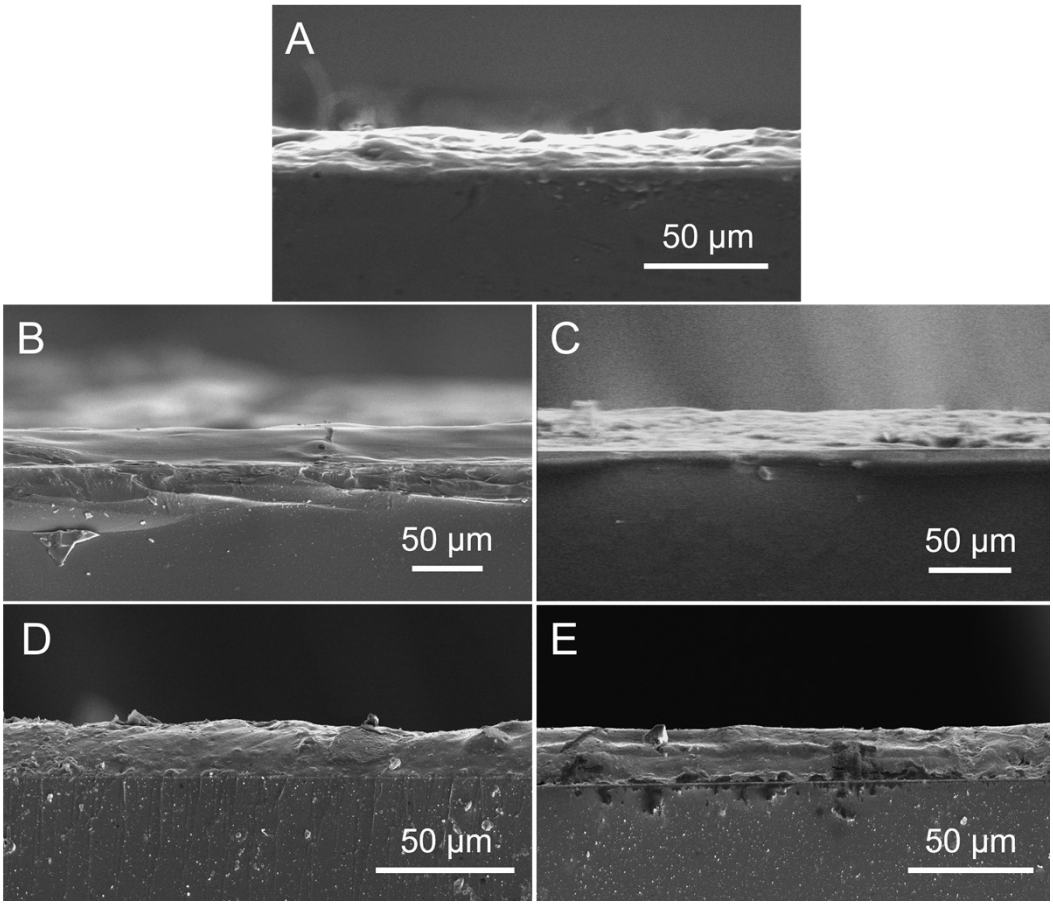

Fig. S8 Cross-sectional SEM images showing the film thicknesses of (A) AuNPs, (B) P3HT, (C) P3HT/AuNPs, (D) PTh-PDI-DCP and (E) PTh-PDI-DCP/AuNPs thin films.

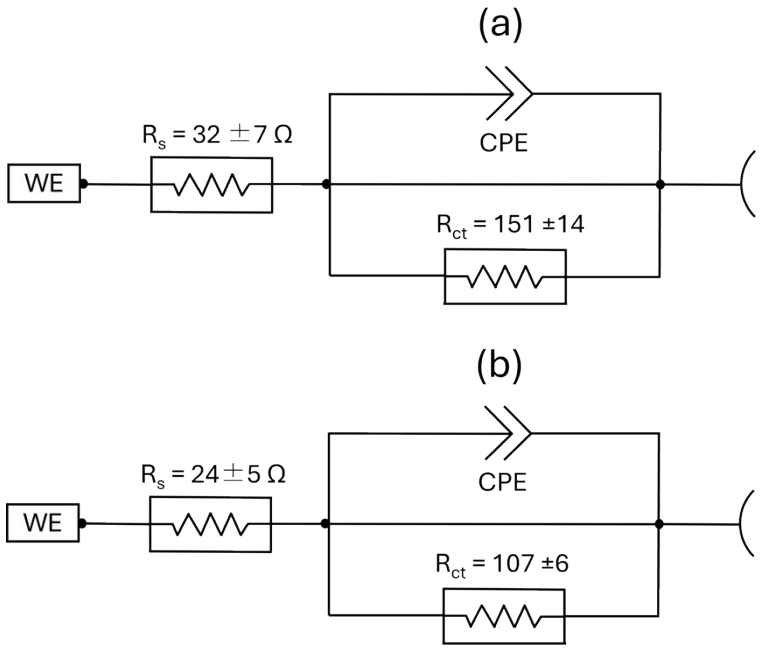

Fig. S9 Diagramatical representation of EIS circuit fiting from Nyquist plots (Fig. 3f) for the PTh-PDI-DCP/AuNPs in the dark (a) and under illumination (b).

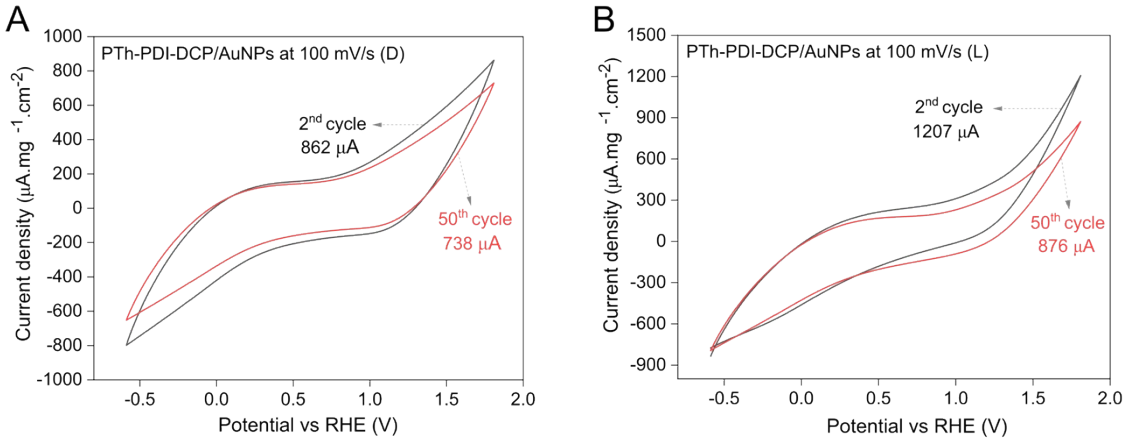

Fig. S10 CVs of the PTh-PDI-DCP/AuNPs hybrid after 50 consecutive cycles recorded in the dark (A) and under illumination (B) which reveal a decrease in current density of ~14% and 27%, respectively, indicating the PTh-PDI-DCP/AuNPs hybrid performance degradation under both conditions.

4. Photocatalytic H_2O_2 production

Photocatalysts were loaded onto PVDF membranes following a previously reported protocol.[1] Photocatalytic activity was evaluated in a 25 mL single-neck round-bottom flask (RBF). A PVDF membrane coated with 0.5 mg of photocatalyst (dispersed in 300 µL of $CHCl_3$) and attached to a magnetic stirrer was placed in the flask, followed by the addition of 5 mL of DI water. The system was sealed with a rubber septum and purged with oxygen for 30 min prior to illumination. Photocatalytic reactions were conducted under Xe lamp (H11 xenon-simulated, high-performance halogen filament bulb, 75 W, 12 V), delivering a light intensity of 60 mW/cm^2 as measured with a flux meter, operated at full intensity for 1 h with continuous stirring. After irradiation, the photocatalyst-coated membrane was removed, thoroughly rinsed with DI water, and dried at 70 °C for subsequent reuse.

Quantification of hydrogen peroxide (H_2O_2) was performed *via* iodometric titration. Briefly, 1 mL of 0.1 M potassium hydrogen phthalate (KHP) solution and 1 mL of 0.4 M potassium iodide (KI) solution were added to the reaction flask. The mixture was stirred at room temperature for 30 min during which photocatalytically generated H_2O_2 oxidized iodide (I^-) to triiodide (I_3^-) under acidic conditions according to Eq. S3:

$$H_2O_2 + 3I^- + 2H^+ \longrightarrow I_3^- + 2H_2O \quad \text{..... Eq. S3}$$

The concentration of I_3^- was determined by measuring its characteristic absorbance at 352 nm using UV/Vis spectroscopy. The corresponding H_2O_2 concentration was calculated from a calibration curve prepared using standard H_2O_2 solutions (0-100 µM) derived from a 35% w/w commercial stock (Fig. S12). For mechanistic studies of H_2O_2 production, four photocatalyst-loaded PVDF membranes (weighed before and after loading using a Mettler Toledo METT-XPR36 microbalance), were individually placed in 25 mL RBFs containing 5 mL of DI water. Specific scavengers were introduced into separate flasks: *tert*-butanol (1 mL, 10 vol.%) as a hydroxyl radical scavenger, *para*-benzoquinone (*p*-BQ, 1 mL, 0.1 mM) to quench superoxide radicals ($^{\bullet}O_2^-$) and $AgNO_3$ (1 mL, 1 mM) as an electron scavenger. One flask without any scavenger served as a control. All systems were purged with oxygen for 30 min and irradiated under the Xe-lamp for 1 h with continuous stirring. After illumination, the membranes were removed, and iodometric reagents (0.1 M KHP and 0.4 M KI) were added. Following 30 min of stirring at room temperature, absorbance at 352 nm was recorded and H_2O_2 production was quantified against the calibration curve. This protocol enabled reproducible quantification of H_2O_2 generation and provided mechanistic insights into the contribution of reactive species in the photocatalytic process highlighting the role of scavengers in elucidating electron, superoxide and hydroxyl radical pathways.

5. ATR-FTIR spectra of the photocatalysts loaded on PVDF membranes

ATR-FTIR spectra of pristine PVDF membranes and photocatalyst-loaded PVDF membranes (AuNPs, P3HT, P3HT/AuNPs, PTh-PDI-DCP, and PTh-PDI-DCP/AuNPs) were recorded (Fig. S11). In the pristine PVDF membrane, characteristic absorption bands at 1166 cm^{-1} and 1233 cm^{-1} were assigned to C-F and C-CF_2 stretching vibrations, respectively. Upon incorporation of the photocatalysts, these bands decreased in intensity, while new absorption features corresponding to the chemical functionalities of the respective photocatalysts emerged. Notably, bands in the 2800-3000 cm^{-1} region, attributed to C-H stretching vibrations and a distinct band near 1700 cm^{-1}, corresponding to the carbonyl (>C=O) stretching mode, confirmed successful deposition of the photocatalyst on the PVDF surface. The relatively low photocatalyst loading (~0.1 mg) resulted in these characteristic peaks appearing with reduced intensity.

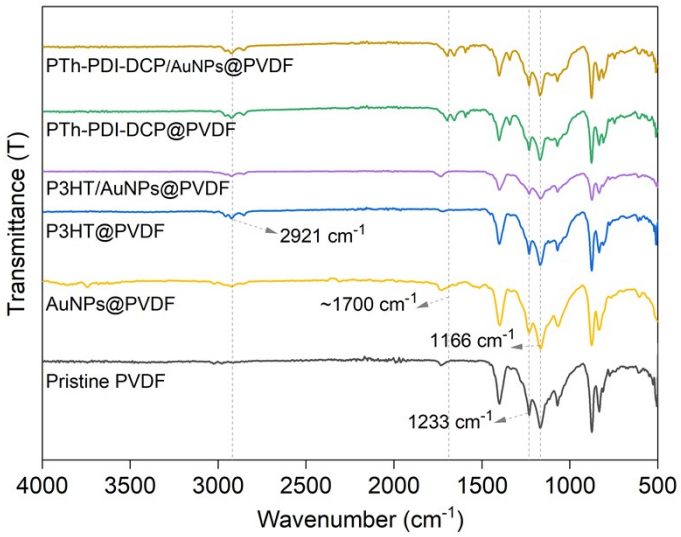

Fig. S11 ATR-FTIR spectra of pristine porous PVDF membrane and PVDF membranes loaded with AuNPs, P3HT, P3HT/AuNPs, PTh-PDI-DCP and PTh-PDI-DCP/AuNPs.

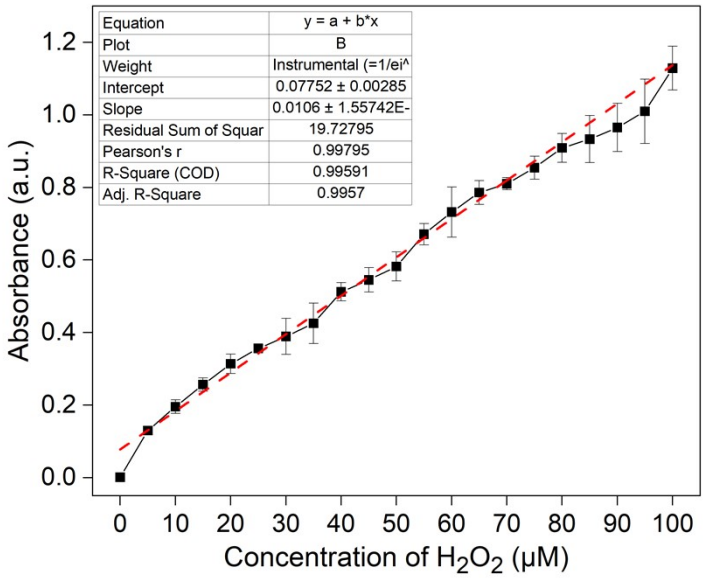

Fig. S12 Calibration curve generated using known molar concentrations prepared from a 35% commercially available H_2O_2 solution.

Table S2 H_2O_2 is produced ($\mu Mmg^{-1}h^{-1}$) by each photocatalyst over 10 photocatalytic cycles in triplicate.

Photocatalyst	No.	AMOUNT LOADED (MG)	1	2	3	4	5	6	7	8	9	10
AuNPs	1	0.11	57	40	35	44	42	34	39	31	28	35
	2	0.12	66	40	39	63	53	38	41	34	30	34
	3	0.12	51	41	48	51	45	36	36	37	34	43
Average H_2O_2			61	40	41	52	46	36	39	34	30	37
SD (±)			6	1	5	8	5	2	2	3	2	4
P3HT	1	0.12	66	74	103	81	84	88	56	60	48	43
	2	0.11	61	76	97	84	73	55	55	60	50	31
	3	0.11	68	72	107	81	88	75	51	57	46	37
Average H_2O_2			65	74	102	82	82	73	54	59	48	37
SD (±)			3	2	4	2	7	13	2	1	2	5
P3HT/AuNPs	1	0.12	94	135	168	108	116	93	70	85	60	64
	2	0.11	88	135	157	102	113	91	61	70	60	68
	3	0.11	99	126	171	98	108	100	65	73	54	68
Average H_2O_2			94	132	165	102	112	95	65	76	58	67
SD (±)			4	4	6	4	3	4	4	6	3	2
PTh-PDI-DCP	1	0.13	90	138	165	142	137	102	67	72	72	52
	2	0.11	97	160	172	138	125	117	61	73	82	56
	3	0.14	107	171	173	172	127	112	67	73	75	57
Average H_2O_2			98	157	170	151	130	111	65	73	75	55
SD (±)			7	14	4	15	5	6	3	2	5	2
PTh-PDI-DCP/AuNP	1	0.13	157	185	245	183	152	114	81	92	101	69
	2	0.10	122	160	238	181	157	126	80	101	116	77
	3	0.12	107	191	216	181	148	114	80	86	104	70

Average H_2O_2			129	178	233	182	152	118	80	93	107	72
SD (±)			21	13	12	1	4	6	0	6	7	4

Table S3 Mechanistic studies for the artificial photosynthesis of H_2O_2 during 5 repeated cycles in triplicates. Note: P is the photocatalytic production of H_2O_2 in $\mu Mmg^{-1}h^{-1}$ and M refers to the PVDF membrane.

Photocatalyst	**Scavenger**	**Amount loaded (mg)**	**(P1)**	**(P2)**	**(P3)**	**(P4)**	**(P5)**	**(P_{av})**
AuNPs	without scavenger	0.12	21	21	15	16	16	18
	$AgNO_3$	0.11	7	7	7	7	7	7
	p-BQ	0.11	10	12	8	11	10	10
	tert-BuOH	0.12	20	19	15	13	13	16
P3HT	without scavenger	0.10	22	29	39	32	24	29
	$AgNO_3$	0.12	9	9	19	11	7	11
	p-BQ	0.11	18	20	33	25	20	23
	tert-BuOH	0.10	19	22	34	27	23	25
P3HT/AuNPs	without scavenger	0.10	32	50	70	43	32	45
	$AgNO_3$	0.11	13	15	24	16	11	16
	p-BQ	0.11	21	31	39	25	15	26
	tert-BuOH	0.10	25	43	58	33	29	38
PTh-PDI-DCP	without scavenger	0.10	36	67	83	41	39	53
	$AgNO_3$	0.11	15	30	29	20	22	23
	p-BQ	0.11	25	47	48	27	24	34
	tert-BuOH	0.11	25	42	42	23	27	32
PTh-PDI-DCP/AuNPs	without scavenger	0.10	62	135	180	100	67	109
	$AgNO_3$	0.11	22	41	40	31	26	32
	p-BQ	0.12	26	76	85	51	35	55
	tert-BuOH	0.11	35	80	97	51	40	61

Table S4 The percentage (%) decrease in H_2O_2 concentration was determined based on mechanistic studies of H_2O_2. Note: % refers to decrease in the photocatalytic production of H_2O_2 and M refers to the PVDF membrane.

Photocatalyst	Scavenger	(%-1)	(%-2)	(%-3)	(%-4)	(%-5)	$\%_{av}$ + SD
AuNPs	without scavenger						
	$AgNO_3$	65	69	55	57	60	61 ±5
	p-BQ	51	42	49	33	40	43 ±6
	tert-BuOH	4	12	4	18	18	11 ±6
P3HT	without scavenger						
	$AgNO_3$	62	67	51	66	70	63 ±7
	p-BQ	18	28	15	20	18	20 ±5
	tert-BuOH	13	22	12	14	2	13 ±6
P3HT/AuNPs	without scavenger						
	$AgNO_3$	59	71	65	64	65	65 ±4
	p-BQ	33	37	44	43	55	42 ±7
	tert-BuOH	20	14	18	24	8	17 ±5
PTh-PDI-DCP	without scavenger						
	$AgNO_3$	59	56	65	50	44	55 ±7
	p-BQ	31	30	43	35	39	36 ±5
	tert-BuOH	31	37	50	44	32	39 ±7
PTh-PDI-DCP/AuNPs	without scavenger						
	$AgNO_3$	65	70	78	69	61	68 ±5
	p-BQ	58	44	53	49	47	50 ±5
	tert-BuOH	43	41	46	49	40	44 ±3

Table S5 List of reported photocatalysts and their photocatalytic activity for the hydrogen peroxide (H_2O_2) production.

Catalyst	Catalyst Loading	Irradiation Source	Irradiation time	H_2O_2 production (reported units)	H_2O_2 production (In $\mu M.mg^{-1}.h^{-1}$)	Reference
RF-P3HT (doping)	50 mg / 30 mL water	Xe lamp, light intensity at 420−700 nm: 210 Wm^{-2}	6 h	98 µmol	10.9	Reference[2]
Rf@ NF 1.0 (resin)	50 mg / 30 mL water	λ > 420 nm (SS-1 Sun)	24 h	186 µmol	5.2	Reference[3]
COF-TfpBpy	15 mg / 10 mL water	λ>420 nm (298 K; xenon lamp, 40.8 mW cm^{-2})	1 h	710 µmol	4733	Reference[4]
COF- UCN-DTDA	20 mg / 20mL water	SS (1-Sun)	1 h	7.3 $mmolg^{-1}$	365	Reference[5]
g-C_3N_4/500-85 °C	30 mg / 30 mL water	Xe (visible light)	7 h	213 µmol	33.8	Reference[6]

g-C_3N_4 (CNOP)	20 mg / 40 mL water	300-W Xe arc lamp (Oriel)	12 h	316 µmol	32.9	Reference[7]
g-C_3N_4/PDI	50 mg / 30 mL water	2 kW Xe lamp (USHIO Inc.)	12 h	42 µmol	2.4	Reference[8]
g-C_3N_4/BDI_{50}	100 mg	Xe-lamp 27.3 $W.m^{-2}$	36 h	118 µmol	1.9	Reference[9, 10]
g-C_3N_4/PDI/rGO	50 mg / 30 mL water	Xe lamp, light intensity 43.3 $W.m^{-2}$	24 h	28 µmol	0.8	Reference[11]
C-modified g-C_3N_4	30 mg / 30mL water	300 W Xenon lamp	2 h	210 µmol	116.6	Reference[12]
Ti_3C_2/g-C_3N_4	50 mg / 50 mL water	300 W Xe-lamp	1 h	140 µmol	56	Reference[13]
CDs/HgL1	10 mg / 50 mL water for 4 h	Xe (350 W)	1 h	800 $\mu molh^{-1}g^{-1}$	1.6	Reference[14]
CdS-PDA	100 mg / 95 mL water	Xe lamp (λ > 420 nm)	24 h	3.84 mM	16.8	Reference[15]
CN/rGO@BPODs	100 mg / 100 mL water	300 W Xe-lamp	1 h	60.6 µmol	6.1	Reference[16]
g-C_3N_4/PDI-$BN_{0.2}$-$rGO_{0.05}$	250 mg / 50 mL water	irradiation of AM 1.5 G simulated sunlight	1 h	26 µmol	2.1	Reference[8]
GO	32 mg / 100 mL water	1.5 kW xenon arc lamp	6 h	202 µmol	10.5	Reference[17]
g-C_3N_4/MTI	100 mg in 100 mL water	solar simulator under AM 1.5G (1-sun)	58 h	52 $\mu molh^{-1}$	5.2	Reference[10]
P3HT 7.0 pH	0.4 mL NPs sol / 30 nmols in water	SS (1-Sun)	20 h	99 µmol	4.95 $\mu mol.h^{-1}$	Reference[18]
CoPc-BTM-COF	100 mg / 50 mL water	AM 1.5 G (SS)	1 h	1250 µmol	250	Reference[19]
CHF-DPDA	In 100 mL water	visible-light irradiation (λ > 420 nm)	16 h	69 $\mu molh^{-1}$	690	Reference[20]
TTF-BT-COF	In 100 mL water	AM 1.5 G sunlight	1 h	276 000 $\mu Mh^{-1}g^{-1}$	276	Reference[21]
CTF-BDDBN	30 mg / 50 mL water	AM1.5G sunlight irradiation (λ > 420 nm)	24 h	82 µM	2.27	Reference[22]
pTh-BTD/FTO	electrodeposited material	Irradiation (100 $mW.cm^{-2}$)	8 h (photo-electrolysis)	~ 3000 µM	375 $\mu M.h^{-1}$	Reference[23]
Nv-CN	50 mL water	AM 1.5 G sunlight	12 h	3093 $\mu molg^{-1}h^{-1}$	5.2	Reference[24]
Anthraquinone-resorcinol	AQ-Re nanoparticles in water	SS (1-Sun)	20 h	6097 $\mu molg^{-1}h^{-1}$	6.1 $\mu mol.mg^{-1}.h^{-1}$	Reference[25]
Pigment semiconductors (EPI), (QNC)	photocathodic H_2O_2 production	60 $mW.cm^{-2}$ light from halogen bulb	48 h	3000 $\mu Mmg^{-1}h^{-1}$	3000	Reference[26]
CoO_x/Mo:$BiVO_4$/Pd	50 mg / 50 mL water	SS (1-Sun)	1 h	58.33 $\mu molg^{-1}h^{-1}$	1.2	Reference[27]
rGO@MRF-x	400 mg / 150 mL water	AM1.5G simulated sunlight (1 sun) irradiation	1 h	481 µmol	8	Reference[28]
G-C_3N_4/500-85˚C/3h	pure water 30 mg / 50 mL water	AM1.5G sunlight irradiation (λ > 420 nm)	7 h	6.4 $\mu Mg^{-1}h^{-1}$	0.0064	Reference[6]
PANI/PDI	10 mg / 1L water	simulated AM1.5G sunlight	1 h	104 $\mu molh^{-1}g^{-1}$	10.4	Reference[29]

Cg-C_3N_4	20 mg powder dispersed in 15 mL H_2O	visible light irradiation ($\lambda \geq 420$ nm)	3 h	1111.89μmol $h^{-1}g^{-1}$	74.0	Reference[30]
OPCN	In 50 mL (25 mg PC) water (2,4-dichlorophenol SA)	AM1.5G sunlight irradiation ($\lambda >$ 420 nm)	1 h	360 $\mu molh^{-1}g^{-1}$	7.2	Reference[31]
Polymer (DE7)	5 mg catalyst in 3 mL water	simulated AM1.5G sunlight	1 h	1190 $\mu molh^{-1}g^{-1}$	396	Reference[32]
Ni-CAT-CN60	In pure water	300 W Xe-lamp	4 h	110 $\mu Mg^{-1}h^{-1}$	0.11	Reference[33]
(MTI), (BDI), (BDI), PDI	In 50 mL water	Xe lamp (100 W)	1 h	10 $\mu molh^{-1}g^{-1}$ - 1610 $\mu molh^{-1}g^{-1}$	0.2 - 32.2	Reference[18]
(CHFs),DPDA	In 50 mL water	AM1.5G sunlight irradiation ($\lambda >$ 420 nm)	1 h	1733 $\mu molh^{-1}g^{-1}$	34.7	Reference[20]
PTA0.6/CN	50 mg / 30 mL water	SS (1-Sun)	12 h	1833 $\mu mol\ g^{-1}\ h^{-1}$	61.1	Reference[34]
Polyethylenimine/g-C_3N_4	In water 10 mL / 10 mg catalyst	$\lambda >$ 420 nm (SS-1sun)	1 h	60 $\mu Mg^{-1}h^{-1}$	0.06	Reference[35]
RF-$(COOH)_2$-523	50 mg / 30 mL water	visible-light irradiation ($\lambda >$ 420 nm)	24 h	60 μmol	1.7	Reference[36]
RF-NH_3-523	In DI water	SS (1-Sun)	8 h	108 $\mu Mg^{-1}h^{-1}$	0.11	Reference[37]
CdS/COF	2 mg/mL of water	simulated sunlight or visible light ($\lambda \geq$ 400 nm)	6 h	608.41 $\mu molL^{-1}$	50.7	Reference[38]
rGO/TiO_2 (10 wt%)	0.5 g/L of photocatalyst, 5 vol% of 2-propanol, pH = 3.0	UV light irradiation ($\lambda \geq$ 320 nm)	3 h	889 $\mu molg^{-1}h^{-1}$	8.89	Reference[39]
PTh-PDI-DCP	~0.1 mg catalyst loaded on porous hydrophobic PVDF membrane / 5 mL water	Xe-lamp white-blue light with light intensity ~100 $mWcm^{-2}$	1 h	215.8 $\mu Mmg^{-1}h^{-1}$	215.8	Reference[1]
P3HT-*b*-poly(3HT-*co*-Th/PDI)	~0.1 mg catalyst loaded on porous hydrophobic PVDF membrane / 5 mL water	Xe-lamp (250-850 nm), (75 W), light intensity ~60 $mWcm^{-2}$	1 h	122.5 $\mu Mmg^{-1}h^{-1}$	122.5	Reference[40]
PTh-PDI-DCP	~0.1 mg catalyst loaded on porous hydrophobic PVDF membrane / 5 mL water	Xe-lamp (250-850 nm), (75 W), light intensity ~60 $mWcm^{-2}$	1 h	120.4 $\mu Mmg^{-1}h^{-1}$	120.4	**Our work**
PTh-PDI-DCP/rGO	~0.1 mg catalyst loaded on porous hydrophobic PVDF membrane / 5 mL water	Xe-lamp (250-850 nm), (75 W), light intensity ~60 $mWcm^{-2}$	1 h	193.6 $\mu Mmg^{-1}h^{-1}$	193.6	**Our work**
PTh-PDI-DCP/AuNPs	~0.1 mg catalyst loaded on porous hydrophobic PVDF membrane / 5 mL water	Xe-lamp (250-850 nm), (75 W), light intensity ~60 $mWcm^{-2}$	1 h	233 $\mu Mmg^{-1}h^{-1}$	233	**This work**

6. References

1. S. Iqbal, F. Akbar, M. A. Salar, T. S. Butt, A. A. Khan, M. Sohail and B. Yameen, *ACS Applied Materials & Interfaces*, 2025, **17**, 28609-28621.
2. Y. Shiraishi, M. Matsumoto, S. Ichikawa, S. Tanaka and T. Hirai, *Journal of the American Chemical Society*, 2021, **143**, 12590-12599.
3. Y. Shiraishi, M. Jio, K. Yoshida, Y. Nishiyama, S. Ichikawa, S. Tanaka and T. Hirai, *JACS Au*, 2023, **3**, 2237-2246.
4. M. Kou, Y. Wang, Y. Xu, L. Ye, Y. Huang, B. Jia, H. Li, J. Ren, Y. Deng and J. Chen, *Angewandte Chemie International Edition*, 2022, **61**, e202200413.
5. P. Sha, L. Huang, J. Zhao, Z. Wu, Q. Wang, L. Li, D. Bu and S. Huang, *ACS Catalysis*, 2023, **13**, 10474-10486.
6. B. Liu, J. Du, G. Ke, B. Jia, Y. Huang, H. He, Y. Zhou and Z. Zou, *Advanced Functional Materials*, 2022, **32**, 2111125.
7. L. Sun, P. Li, Z. Shen, Y. Pang, X. Ma, D. Qu, L. An and Z. Sun, *Advanced Energy and Sustainability Research*, 2023, **4**, 2300090.
8. Y. Kofuji, Y. Isobe, Y. Shiraishi, H. Sakamoto, S. Ichikawa, S. Tanaka and T. Hirai, *ChemCatChem*, 2018, **10**, 2070-2077.
9. S. Chu, Y. Pan, Y. Wang, H. Zhang, R. Xiao and Z. Zou, *Journal of Materials Chemistry A*, 2020, **8**, 14441-14462.
10. Y. Kofuji, S. Ohkita, Y. Shiraishi, H. Sakamoto, S. Ichikawa, S. Tanaka and T. Hirai, *ACS Sustainable Chemistry & Engineering*, 2017, **5**, 6478-6485.
11. Y. Kofuji, Y. Isobe, Y. Shiraishi, H. Sakamoto, S. Tanaka, S. Ichikawa and T. Hirai, *Journal of the American Chemical Society*, 2016, **138**, 10019-10025.
12. T. Wang, N. Song, S. Yao, Y. Wang, Q. Wang and H. Yu, *Chemical Engineering Journal*, 2024, **495**, 153379.
13. Y. Yang, Z. Zeng, G. Zeng, D. Huang, R. Xiao, C. Zhang, C. Zhou, W. Xiong, W. Wang and M. Cheng, *Applied Catalysis B: Environmental*, 2019, **258**, 117956.
14. Y. Zhao, L. Xu, X. Wang, Z. Wang, Y. Liu, Y. Wang, Q. Wang, Z. Wang, H. Huang and Y. Liu, *Nano Today*, 2022, **43**, 101428.
15. Z. Wei, S. Zhao, W. Li, X. Zhao, C. Chen, D. L. Phillips, Y. Zhu and W. Choi, *ACS Catalysis*, 2022, **12**, 11436-11443.
16. J. Xiong, X. Li, J. Huang, X. Gao, Z. Chen, J. Liu, H. Li, B. Kang, W. Yao and Y. Zhu, *Applied Catalysis B: Environmental*, 2020, **266**, 118602.
17. W.-C. Hou and Y.-S. Wang, *ACS Sustainable Chemistry & Engineering*, 2017, **5**, 2994-3001.
18. H. Cheng, J. Cheng, L. Wang and H. Xu, *Chemistry of Materials*, 2022, **34**, 4259-4273.
19. Q. Zhi, W. Liu, R. Jiang, X. Zhan, Y. Jin, X. Chen, X. Yang, K. Wang, W. Cao and D. Qi, *Journal of the American Chemical Society*, 2022, **144**, 21328-21336.
20. H. Cheng, H. Lv, J. Cheng, L. Wang, X. Wu and H. Xu, *Advanced Materials*, 2022, **34**, 2107480.
21. J. N. Chang, Q. Li, J. W. Shi, M. Zhang, L. Zhang, S. Li, Y. Chen, S. L. Li and Y. Q. Lan, *Angewandte Chemie*, 2023, **135**, e202218868.
22. L. Chen, L. Wang, Y. Wan, Y. Zhang, Z. Qi, X. Wu and H. Xu, *Advanced Materials*, 2020, **32**, 1904433.
23. R. Gańczarczyk, R. Rybakiewicz-Sekita, M. Gryszel, J. Drapała, M. Zagórska and E. D. Głowacki, *Advanced Materials Interfaces*, 2023, **10**, 2300270.
24. R. Ji, Y. Dong, X. Sun, C. Pan, Y. Yang, H. Zhao and Y. Zhu, *Applied Catalysis B: Environment and Energy*, 2024, **349**, 123884.
25. A. V. Munde, D. M. Sanke, N. G. Ghosh, J. Bezboruah, S. Roy and S. S. Zade, *Journal of Materials Chemistry A*, 2024, **12**, 18433-18439.
26. M. Jakešová, D. H. Apaydin, M. Sytnyk, K. Oppelt, W. Heiss, N. S. Sariciftci and E. D. Głowacki, *Advanced Functional Materials*, 2016, **26**, 5248-5254.

27. A. Turunen, 2023.
28. Q. Tian, X. K. Zeng, C. Zhao, L. Y. Jing, X. W. Zhang and J. Liu, *Advanced Functional Materials*, 2023, **33**, 2213173.
29. W. Dai, L. Jiang, J. Wang, Y. Pu, Y. Zhu, Y. Wang and B. Xiao, *Chemical Engineering Journal*, 2020, **397**, 125476.
30. J. Liang, X. Yang, Y. Wang, P. He, H. Fu, Y. Zhao, Q. Zou and X. An, *Journal of Materials Chemistry A*, 2021, **9**, 12898-12922.
31. F. Wang, J. Xu, Z. Wang, Y. Lou, C. Pan and Y. Zhu, *Applied Catalysis B: Environmental*, 2022, **312**, 121438.
32. L. Liu, M.-Y. Gao, H. Yang, X. Wang, X. Li and A. I. Cooper, *Journal of the American Chemical Society*, 2021, **143**, 19287-19293.
33. Y. Zhao, Y. Liu, Z. Wang, Y. Ma, Y. Zhou, X. Shi, Q. Wu, X. Wang, M. Shao and H. Huang, *Applied Catalysis B: Environmental*, 2021, **289**, 120035.
34. J. Cao, Q. Wu, Y. Zhao, K. Wei, Y. Li, X. Wang, F. Liao, H. Huang, M. Shao and Y. Liu, *Applied Catalysis B: Environmental*, 2021, **285**, 119817.
35. J. Yan, X. Song, B. Jin and R. Peng, *New Journal of Chemistry*, 2021, **45**, 14655-14664.
36. Y. Shiraishi, T. Hagi, M. Matsumoto, S. Tanaka, S. Ichikawa and T. Hirai, *Communications Chemistry*, 2020, **3**, 169.
37. Y. Shiraishi, T. Takii, T. Hagi, S. Mori, Y. Kofuji, Y. Kitagawa, S. Tanaka, S. Ichikawa and T. Hirai, *Nature materials*, 2019, **18**, 985-993.
38. Y. He, J. Zhao, Y.-T. Sham, S. Gao, M. Pan, Q. Chen, G. Huang, P. K. Wong and J. Bi, *ACS Sustainable Chemistry & Engineering*, 2023, **11**, 17552-17563.
39. D. Kong, M. Zhao, S. Li, F. Huang, J. Song, Y. Yuan, Y. Shen and A. Xie, *Nano*, 2016, **11**, 1650007.
40. F. Akbar, S. Iqbal, A. Sohail, S. Çitoğlu, H. Duran and B. Yameen, *ACS Applied Energy Materials*, 2025.